Fast and Efficient Clutter Cancellation Approach for DVB-T Based Passive Radars

Mohamed E. Nouar[1, *], Osama Mahfoudia[1], Azzedine Bouaraba[1], and Xavier Neyt[2]

Abstract—In passive radar systems, target echoes are submerged in the sidelobes of the static clutter, which includes multiple reflection echoes from the objects located in the operating environment of the considered system. This undesired part of the collected signals degrades the detector performances. Consequently, the reduction of the static clutter contribution is essential to ensuring an efficient operation of passive radars. In the literature, many algorithms and methods have been proposed for clutter suppression, where a high quality of the received signals is required to ensure an efficient clutter suppression. These methods require a considerable amount of data to operate which increases the complexity and the calculation load of the algorithms. In this paper, an important contribution is brought by simultaneously improving the signals quality and reducing the calculation load in the static clutter suppression process. Since the static clutter can be considered as time-invariant, the proposed approach exploits the specific architecture of the DVB-T signals to provide a noise reduction in the receiving channels by averaging the received signals after being split into symbols. Three different methods are proposed to examine the efficiency of the proposed approach. The performances of the proposed approach are validated through a set of simulations and verified using real data.

1. INTRODUCTION

Radar systems employ electromagnetic radiation to detect and track targets of interest by evaluating the radar-target propagation delay [1, 2]. An active radar system requires two parts: a transmitter and a receiver. The transmitter generates electromagnetic waves, while the receiver captures eventual target echoes. In contrast, passive coherent location (PCL) radar systems exploit illuminators of opportunity (IOs) to ensure the target detection [3]. Thus, PCL radars operate in an electromagnetic silent mode which offers many advantages such as low cost and the property of being immunized to hostile interception [4, 5].

The illuminators of opportunity are the electromagnetic radiation sources that are exploited as transmitters for PCL radars. In the literature, many of this electromagnetic radiation sources are exploited such as broadcasting and telecommunication transmitters [5]. The most common sources are the frequency modulation (FM) radio [6], global system for mobile communications (GSM) [7], digital audio broadcasting (DAB), and digital video broadcasting-terrestrial (DVB-T) [3, 4, 8]. These radiation sources are not designed to be employed for remote sensing applications. Consequently, the PCL radar performances depend on the parameters of the exploited IO. For example, the transmitter power and signal bandwidth define the maximum detection range and the range resolution, respectively [8].

PCL radars can be bistatic or multistatic [3, 9]; bistatic PCL radars employ one receiver which gather the transmitted signals of one transmitter, while multistatic PCL radars can be seen as a group of receivers and transmitters [4]. The conventional configuration of the bistatic PCL radars is presented in Figure 1; it involves two receiving channels: a reference channel (RC) and a surveillance channel
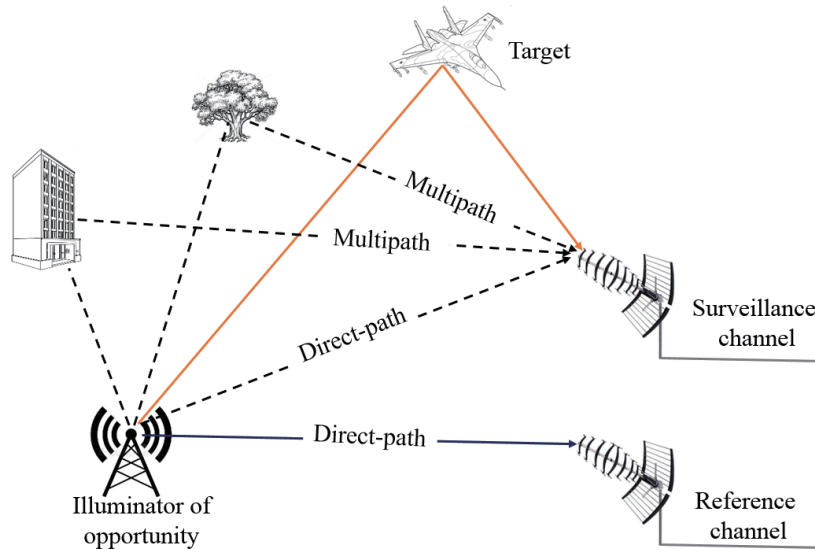
Figure 1. Bistatic PCL radar configuration.

(SC). The RC is pointed towards the illuminator of opportunity site to obtain a noisy version of the transmitted signal called the direct-path signal, and the SC is oriented to the area of interest to collect possible target echoes [8].

In PCL radars, the target detection can be performed through a cross-correlation (CC) detector [10]. The CC detector cross-correlates the surveillance signal and a time-delayed and frequency-shifted copy of the reference signal. The CC detector operates similarly to the matched filter (MF) by employing the received reference signal instead of the exact transmitted signal which is unknown [10]. The reference signal is often corrupted by noise which decreases the coherent integration gain for the CC detector and thus, leads to a degradation of its performance in terms of detection probability compared to the MF. This issue has been addressed in [11, 12] where an assessment of the impact of noise in the reference signal on the detection probability has been carried out employing theoretical analysis.

The DVB-T signals are characterized by a wide bandwidth, a high radiated power, and a thumbtack ambiguity function which represent attractive qualifications for being exploited as illumination sources in PCL radars [11, 13, 14]. In addition, the DVB-T based PCL radars can enhance the signal-to-noise ratio of the received reference signal by demodulating it and reconstructing the resulting symbols [15]. As a result, the DVB-T signals are widely used in the PCL radars [16]. In this work, the bistatic PCL systems based on the DVB-T signals are considered.

In addition to the reflected signal from targets of interest, the surveillance signal contains a direct signal from the illuminator of opportunity and a multipath clutter resulting from the static scatterers in the detection scene such as trees and buildings [7, 17]. Due to their sidelobes effect, the multipath components can mask weak targets and decrease detection performances [3, 18]. Thus, a multipath rejection processing is required to enhance the detection performances. Different approaches are used for clutter cancellation such as adaptive methods [18, 19], sequential algorithms [20–22], and frequency domain methods [23]. The majority of these approaches are based on the projection of the surveillance signal into a subspace which is orthogonal to the direct signal [5, 21].

The adaptive methods are based on the adaptive filter theory such as the least mean square (LMS) algorithm [24]. The resulting filtered signal (after the static clutter suppression) is obtained by subtracting a weighted sum of time-delayed replicas of the reference signal [25, 26] from the surveillance signal. The filter weights are adaptively adjusted to match with the static clutter components [27, 28].

The sequential methods for the static clutter suppression are multistage processes [20, 22, 29], the extensive cancellation algorithm (ECA) and its variants [20, 30, 31], and they detect and suppress the impact of the static clutter from the surveillance signal during a set of iterations until a stopping criterion is reached [5, 22].

Among the exploited IOs, the digital waveform signals such as DVB-T offer the possibility of the static clutter suppression in the frequency domain. An example of methods is the frequency domain analysis cancelation algorithm (FDACA) [32]. The algorithms of this category process the signals in the frequency domain [23, 33, 34], which means that the clutter impact is suppressed by estimating the channel spectral response. The main difference between the algorithms of this category is the considered approach to estimate the propagation channel response.

The most important part of the cancellation process is the estimation of the static clutter components [34, 35]. The accuracy of the clutter estimation depends on the considered number of samples; the more the samples are used, the better the estimation accuracy is [34]. However, many clutter suppression approaches include matrix inversion stages [30]. As a result, a large number of considered samples can significantly increase the calculation load. In addition, the received signals are generally collected with a low signal-to-noise ratio, which negatively impacts the estimation accuracy of these methods [24, 29, 34]. The conventional clutter suppression algorithms consider a large dimension of the received signals, and the performance of these algorithms depends on the quality of the received signals. In addition, signals from the passive radars systems are generally collected with a high noise power, which negatively impacts the estimation accuracy of the of these methods [24, 29, 34].

In this paper, we propose a two-stages approach for the static clutter suppression. The first stage is the preprocessing of the received signals to improve the quality of the received signals and to decrease the size of the needed data to obtain an accurate clutter components estimation. The second stage can be performed by employing any classical clutter suppression with the preprocessed signals as input. This approach provides higher performances than the classic algorithms where no preprocessing is considered, and it reduces the number of samples used for the clutter components estimation and suppression by exploiting the specific structure of the DVB-T signals.

This paper is organized as follows. Section 2 presents the signal model and problem analysis. Section 3 provides the details of the proposed approach. In Section 4, simulation results are presented and discussed. Section 5 involves the experimental results using real data. In Section 6, the paper conclusion is given.

2. SIGNAL MODEL AND PROBLEM ANALYSIS

In this section, the DVB-T structure is described in details, and the specifications that will be exploited in the proposed approach will be emphasized. Then, the mathematical modeling of the received reference and surveillance signals are provided. Finally, the impact of the static clutter on the detection performances will be shown through a simulation example.

2.1. DVB-T Signal Structure

The DVB-T standard employs the Orthogonal Frequency Division Multiplex (OFDM) modulation with two famous transmission modes, 2 K and 8 K. The transmitted signal is constituted of consecutive symbols [14, 36].

Each symbol is formed by a useful part of duration T_U and a guard interval of duration T_G, as illustrated in Figure 2. The guard interval is generated by the cyclic prefix, and its duration can be selected from these four values $T_G \in \{T_U/4, T_U/8, T_U/16, T_U/32\}$ [5, 36]. In this paper, the 8 K mode is used in simulation with $T_G = T_U/4$. We note the full duration of one DVB-T symbol as T_S, which is given by [36, 37]:

$$T_S = T_U + T_G \tag{1}$$

Figure 3 presents the DVB-T frame structure. For each DVB-T symbol and among the totality of N_c subcarriers, three types of data are transported: useful data in N_d subcarriers, transmission parameter signaling (TPS) in N_{TPS} subcarriers, and pilots in N_p subcarriers. Table 1 summarizes the main parameters of the DVB-T signal [14].

The transmitted signal $s(i, n)$ for the ith DVB-T symbol can be expressed as [14]:

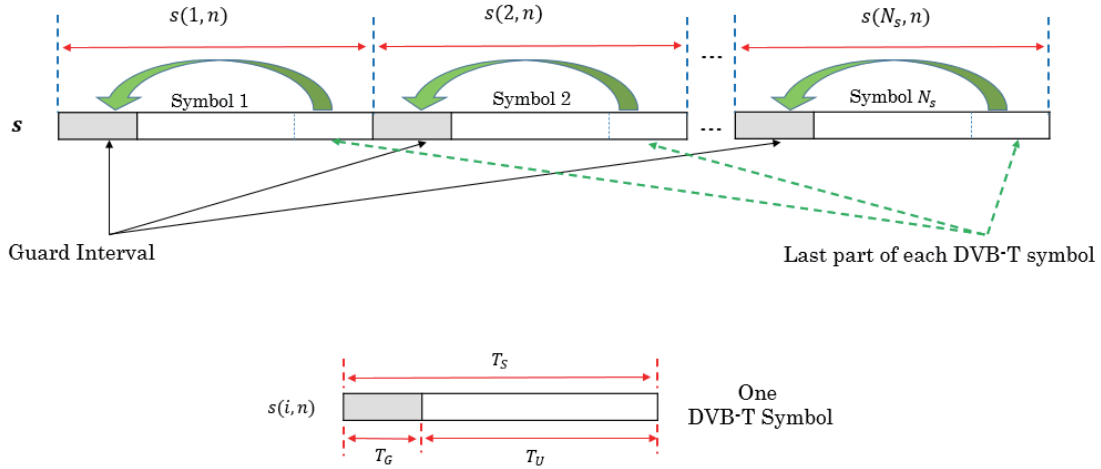$$s(i, n) = \sum_{k=0}^{N_c-1} C_k(i) e^{2j\pi f_k n} \tag{2}$$
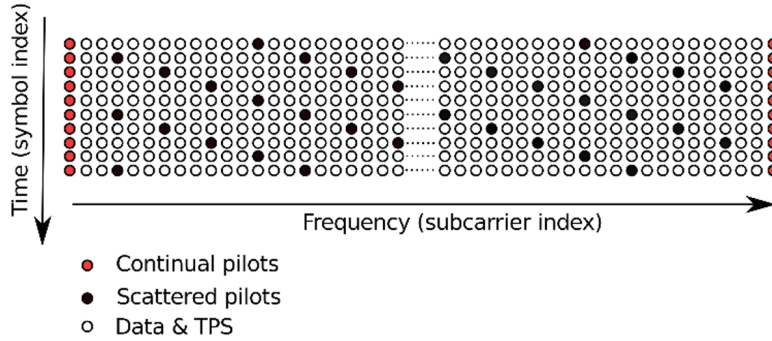
Figure 2. Guard intervals in DVB-T symbols.

Figure 3. DVB-T signal structure [5].

Table 1. Main parameters of DVB-T signal [5].

mode	2 K	8 K
Number of subcarriers N_c	1705	6817
Number of data subcarriers K_d	1512	6048
Number of pilot subcarriers K_p	176	701
Number of TPS subcarriers K_{TPS}	17	68
Useful symbol duration T_U	224 μs	896 μs
Subcarrier spacing ΔF	4464 Hz	1116 Hz
Signal bandwidth B	7.61 MHz	7.61 MHz

where $C_k(i)$ represent the Quadratic Amplitude Modulation (QAM) data, the parameters TPS, or the pilots coefficients, and f_k are the discrete sub-carriers frequencies. The coefficients C_k can be divided into four (04) major parameters [14, 38]:

- D_k for $k \in D$ with D is the domain that contains the indexes of the useful data subcarriers.
- P_k^{TPS} for $k \in T$ with T is the domain that contains the indexes of the TPS subcarriers.
- P_k^{C} for $k \in C$ with C is the domain of the continuous pilot subcarrier indexes occurring in all symbols at the same frequencies [38].

- $P_k{}^S$ for $k \in S$ with S is the domain that contains the indexes of the scattered pilot subcarriers, and their frequencies change from one symbol to another referring to a specific pattern (four (04) symbol periodic) [38].

Equation (2) can be written as follows [38]:

$$s(i, n) = d(i, n) + p_c(n) + p_s(i, n) \tag{3}$$

where $d(n)$ is the sum of data signal and TPS signal with zero mean and a variance of σ_d^2, and $p_c(n)$ involves the continuous pilots signal with zero mean and a variance of $\sigma_{p_c}^2$, whereas $p_s(n)$ is the scattered pilots signal with zero mean and a variance of $\sigma_{p_s}^2$. Since these signals are statistically independent, the variances are related by the expression below:

$$\sigma_s^2 = \sigma_{p_c}^2 + \sigma_{p_s}^2 + \sigma_d^2 \tag{4}$$

2.2. Received Signal Model and Problem Statement

In PCL radar systems and within the single target scenario, the surveillance signal (collected by the SC) is formed by a target echo submerged in noise and mixed with multipath signals, and it can be expressed as follows [36]:

$$x_s(n) = \sum_{l=0}^{L-1} h_l s(n - l) + \alpha s(n - \kappa_0)e^{j2\pi f_d n} + w(n) \tag{5}$$

where L is the number of considered multipath components; each component is characterized by a coefficient h_l and a discrete time delay l; κ_0 and f_d represent the time delay and the Doppler shift caused by the target; α is the target attenuation coefficient. The term $w(n)$ represents the SC complex white gaussian noise with a zero mean and a variance of σ_w^2.

Let us consider the array **h** with:

$$\mathbf{h} = [h_0, h_1, h_2, \ldots, h_{L-1}] \tag{6}$$

which represents the clutter array containing the multipath components, with L being the maximum clutter size.

In this work, we consider that the static clutter contribution is time invariant [34]. Thus, the estimation and cancellation of its effect can be performed in a primary stage before proceeding to the target detection. It follows that without a loss of generality we can consider the following expression of the received surveillance signal in the absence of the target echo:

$$x_s(n) = \sum_{l=0}^{L-1} h_l s(n - l) + w(n) \tag{7}$$

The expression of the reference signal (received by RC) is presented as follows:

$$x_r(n) = \xi s(n) + v(n) \tag{8}$$

where ξ represents the attenuation factor for the reference channel, and $v(n)$ is complex white Gaussian noise with a zero mean and a variance of σ_v^2.

The two signals are characterized by a clutter to noise ratio (CNR) and a signal to noise ratio (SNR_r), respectively:

$$\text{CNR} = \frac{\sigma_s^2}{\sigma_w^2} \sum_{l=0}^{L-1} |h_l|^2 \tag{9}$$

$$\text{SNR}_r = \frac{\sigma_s^2 |\xi|^2}{\sigma_v^2} \tag{10}$$

To indicate the impact of the multipath contribution, we carry out a qualitative assessment of the cross-correlation detector output result. In order to do so, we generate the range-Doppler diagram

(RDD) with a coherent processing interval of length 0.1 second (which provides $N = 10^6$ samples). The expression of the cross-correlation function is given by:

$$\Psi_{CC}(\kappa, \nu) = \sum_{n=0}^{N-1} |x_s(n) \times x_r{}^*(n - \kappa) \times e^{-j2\pi\nu n}|^2 \tag{11}$$

Figure 4 shows the results of a simulated scenario of one target located at a bistatic distance of 2 km with a Doppler shift of 75 Hz under two cases. The first case considers the presence of a static clutter with CNR of 25 dB, and the second case is clutter-free. In both cases, the target echo is characterized by an SNR$_r$ of 20 dB. Figure 4(a) presents the resulting Range-Doppler diagram (RDD) of the first case. In fact, the static clutter (shown here around 0 Hz axis) covers most of the RDD, which masks the target echo. Figure 4(b) shows the resulting RDD for the clutter-free case; the target can be easily distinguished from the noise floor, and thus, can be easily detected. In Figure 4(c), a one-dimensional cut of the previous two RDDs at the target location is shown. This figure demonstrates that the static clutter masks the target echo by the resulting sidelobes. Thus, a degradation of the detection performances is to be expected in the presence of the static clutter.
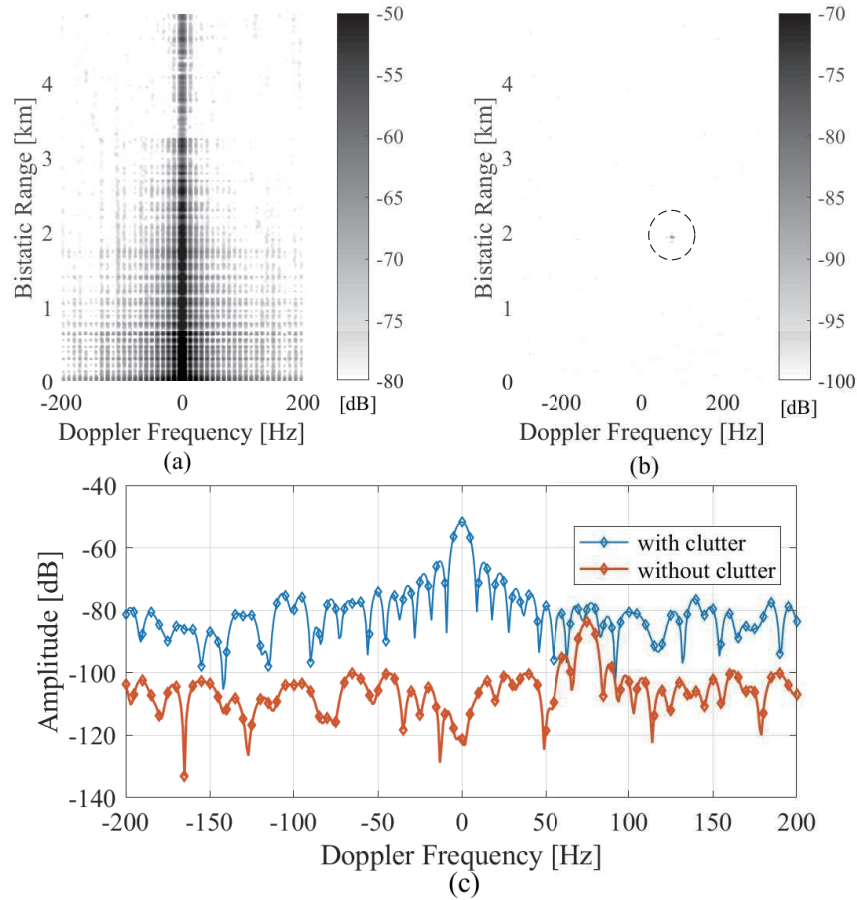

Figure 4. Impact of the static clutter on the target detection. (a) RDD contains static clutter, (b) RDD without clutter contribution, (c) RDD in target range cut for the two scenarios.

3. PROPOSED APPROACH

In this paper, the proposed approach simultaneously deals with the two major issues in the static clutter suppression process: the signals quality and the calculation load. In order to do so, an adaptation of the
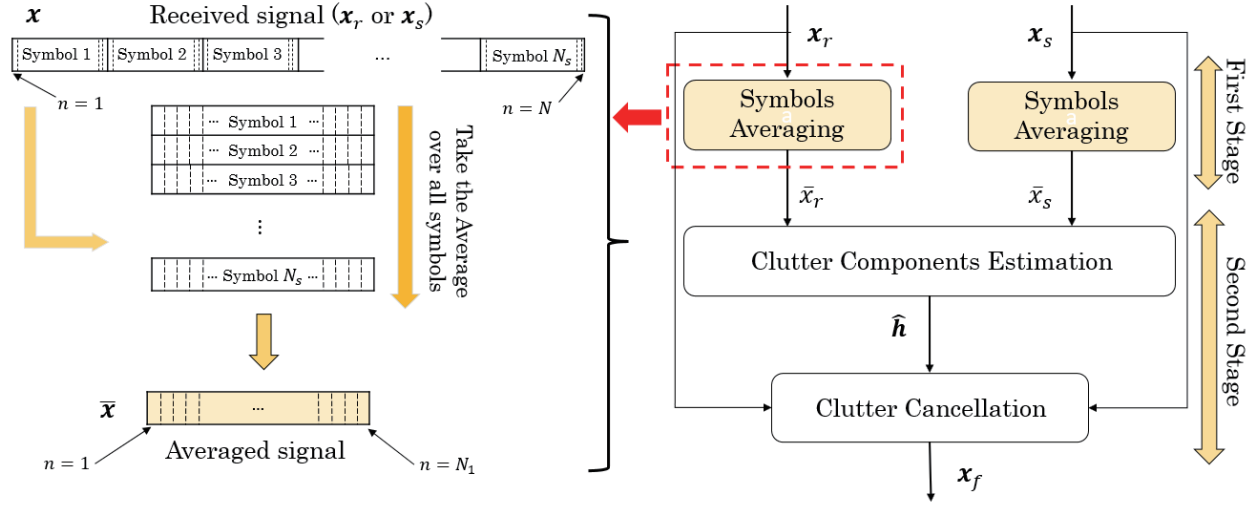
Figure 5. Scheme of the proposed approach.

clutter estimation methods is proposed. It is worth to mention that the proposed approach is dedicated to DVB-T based PCL radars. Figure 5 represents the scheme of the proposed approach which consists of two stages. The first stage is the averaging of the received reference and surveillance signals after they are split into batches of the length of one DVB-T symbol. The averaging process reduces the noise power in the resulting signals and thus, improves the SNRr and CNR parameters. As a result, an improvement of the static clutter estimation will be obtained. The second stage is executed through the application of one classical static clutter method (LMS, ECA, FDACA, ...) on the averaged signals.

3.1. First Stage: Preprocessing

As mentioned in Section 2, the DVB-T signal can be time-divided into independent symbols. The proposed method performs an averaging among N_s DVB-T symbols to obtain one symbol with the minimum of noise-floor level. The expression of the ith symbol of the received surveillance signal is expressed as:

$$x_s(i, n) = \sum_{l=0}^{L-1} h_l s(i, n-l) + w(i, n) \tag{12}$$

and the corresponding reference signal is given by:

$$x_r(i, n) = \xi s(i, n) + v(i, n) \tag{13}$$

Since the noise distribution follows a complex Gaussian model with zero mean and a considered variance, taking the average among N_s DVB-T symbols reduces the noise variance by a factor of $1/N_s$ without losing the useful data. Thus, we note the averaged reference and surveillance signals as $\bar{x}_r(n)$ and $\bar{x}_s(n)$, respectively. By considering the averaging operator $E\{\cdot\}$, the averaged signals are defined as:

$$\bar{x}_r(n) = E\{x_r(i, n)\} \tag{14}$$

$$\bar{x}_s(n) = E\{x_s(i, n)\} \tag{15}$$

Using Equations (12) and (13), we can write $\bar{x}_r(n)$ and $\bar{x}_s(n)$ as follows:

$$\bar{x}_r(n) = \xi E\{s(i, n)\} + E\{v(i, n)\} \tag{16}$$

$$\bar{x}_s(n) = \sum_{l=0}^{L-1} h_l E\{s(i, n-l)\} + E\{w(i, n)\} \tag{17}$$

Now, it is important to calculate the averaged value of the DVB-T symbols $\bar{s}(n) = E\{s(i, n)\}$. Using Equation (3), we can write:

$$\bar{s}(n) = E\{p_c(n)\} + E\{p_s(i, n) + E\{d(i, n)\} \tag{18}$$

If we consider the averaged signal of the scattered pilots as $\bar{p}_s(n) = E\{p_s(i,n)\}$ and the averaged data signal as $\bar{d}(n) = E\{d(i,n)\}$, it follows that:

$$\bar{s}(n) = p_c(n) + \bar{p}_s(n) + \bar{d}(n) \tag{19}$$

with the new expression of $\bar{s}(n)$, the averaged reference and surveillance signals can be expressed as:

$$\bar{x}_r(n) = \xi(p_c(n) + \bar{p}_s(n) + \bar{d}(n)) + \bar{v}(n) \tag{20}$$

and:

$$\bar{x}_s(n) = \sum_{l=0}^{L-1} h_l(p_c(n-l) + \bar{p}_s(n-l) + \bar{d}(n-l)) + \bar{w}(n) \tag{21}$$

with $\bar{v}(n) = E\{v(i,n)\}$ and $\bar{w}(n) = E\{w(i,n)\}$ being the residual noises after the averaging operation:

$$\bar{x}_r(n) = \xi(E\{p_c(n)\} + E\{p_s(i,n) + E\{d(i,n)\}) + E\{v(i,n)\} \tag{22}$$

we put:

$$\bar{p}_s(n) = E\{p_s(i,n)\} \tag{23}$$

Since the noise signals $w(n)$ and $v(n)$ and data signal $d(n)$ are complex additive white Gaussian noise ($CAWGN$), we have:

$$E\{w(i,n) = E\{d(i,n)\}) = E\{v(i,n)\} = 0 \tag{24}$$

When we increase the size of the collected data, the averaging operation reduces the noise enormously, and besides, the scattered pilot signals are repeated every multiple of four (04) symbols, so we realize that:

$$\bar{x}_r(n) = \xi(p_c(n) + \bar{p}_s(n)) \tag{25}$$

from Equation (25) we distinguish the expression of $\bar{x}_s$:

$$\bar{x}_s(n) = \sum_{l=0}^{L-1} h_l(p_c(n-l) + \bar{p}_s(n-l)) \tag{26}$$

and notice that expressions (25) and (26) are verified when we use huge size of received signals, i.e., $i \longrightarrow \infty$, and when we have a limited N_s data size (i.e., $i \in [0,1,\ldots,N_s-1]$) the new expressions of the considered signals are:

$$\bar{x}_r(n) = p_c(n) + \bar{p}_s(n) + \bar{d}(n) + \bar{v}(n) \tag{27}$$

$$\bar{x}_s(n) = \sum_{l=0}^{L-1} h_l(p_c(n-l) + \bar{p}_s(n-l) + \bar{d}(n-l)) + \bar{w}(n) \tag{28}$$

where $\bar{w}(n)$ and $\bar{v}(n)$ are the residual noises after the averaging operation:

$$\bar{w}(n) = \frac{1}{N_s} \sum_{i=0}^{N_s-1} w(i,n) \tag{29}$$

$$\bar{v}(n) = \frac{1}{N_s} \sum_{i=0}^{N_s-1} v(i,n) \tag{30}$$

It is highlighted that the proposed approach significantly reduces the needed storage capacity and the calculation load. In fact, the averaging process requires only the storage space equal to one DVB-T symbol size. In this case, the summation of the considered N_s symbols is performed, and the result is divided by N_s to obtain the averaged signals. For the calculation load, for example the ECA algorithm includes matrix inversion stages, and for a data size of N (typically $N = 10^6$) and a clutter size of L, the size of the matrices to be inverted is $N \times L$. However, the proposed approach offers the reduction of the matrix size to be $N_{symb} \times L$ with N_{symb} the number of samples in one DVB-T signal; here, $N_{symb} = 8192$. Therefore, the important impact on the calculation reduction can be clearly seen in addition to the noise reduction impact.

3.2. Second Stage: Static Clutter Suppression

Once the averaged reference signal $\bar{\mathbf{x}}_\mathbf{r}$ and surveillance signal $\bar{\mathbf{x}}_\mathbf{s}$ are obtained ($N_1 \times 1$ samples), the static clutter suppression can be performed on these two signals. For adaptive methods (such as LMS algorithm), the estimates of the static clutter weights $\hat{\mathbf{h}}$ are obtained through an adaptive process. In this case, the filtered surveillance signal is obtained as followes [27]:

$$x_f^{LMS}(n) = x_s(n) - \sum_{l=0}^{L-1} \hat{h}_l x_r(n-l) \tag{31}$$

The sequential methods, such as ECA algorithms, obtain the static clutter weights $\hat{\mathbf{h}}$ through the least squares approach to minimize the difference between the estimated clutter signal and received surveillance signal, which is expressed as follows [29]:

$$\hat{\mathbf{h}} = (\mathbf{A_1}^H \mathbf{A_1})^{-1} \mathbf{A_1}^H \bar{\mathbf{x}}_\mathbf{s} \tag{32}$$

where A is the matrix given by:

$$\mathbf{A_1} = \mathbf{B}[\mathbf{\Lambda_{-p}} \mathbf{S_r}, \dots, \mathbf{\Lambda_{-1}} \mathbf{S_r}, \mathbf{\Lambda_1} \mathbf{S_r}, \dots, \mathbf{\Lambda_p} \mathbf{S_r}] \tag{33}$$

with $\mathbf{B}$ being an incidence matrix which selects the last N rows of the following matrix and a phase shift which concerns the p$^\text{th}$ Doppler value is applied using the matrix $\mathbf{\Lambda_p}$, while the matrix $\mathbf{S_r}$ is calculated as follows [5]:

$$\mathbf{S_r} = [\bar{\mathbf{x}}_\mathbf{r}, \mathbf{D}\bar{\mathbf{x}}_\mathbf{r}, \mathbf{D}^2 \bar{\mathbf{x}}_\mathbf{r}, \dots, \mathbf{D}^{K_r - 1} \bar{\mathbf{x}}_\mathbf{r}] \tag{34}$$

where $\mathbf{D}$ is a matrix that applies a single sample delay, and K_r is the length of the estimated static clutter vector. The filtered surveillance signal is retrieved as follows:

$$\mathbf{x}_f^{ECA} = \mathbf{x_s} - \mathbf{A}\hat{\mathbf{h}} \tag{35}$$

A is calculated the same as A_1, only here we use x_r instead of $\bar{x}_r$ in Equation (34).

For the frequency domain methods such as FDACA, the static clutter coefficients are estimated in the spectral domain, and they are noted by $\hat{\mathbf{H}}$. To obtain this estimate, the preprocessed surveillance signal undergoes an FFT operation to retrieve its spectral representation $\bar{X}_s$ given by [32]:

$$\bar{X}_s(k) = H(k) C_k + \bar{W}(k) \tag{36}$$

where C_k represents the transmitted QAM symbols, $\bar{W}$ the spectral response of the channel noise, and k the discrete subcarrier frequency index. To perform the static clutter suppression, an estimation of the transmitted QAM signals is required. In order to do so, the preprocessed reference signal $\bar{\mathbf{x}}_\mathbf{r}$ is demodulated to obtain the estimates $\hat{C}_k$. Then, the filtered surveillance signal in the frequency domain is obtained by:

$$X_f^{FDACA}(k) = X_s(k) - \hat{H}(k) \hat{C}_k \tag{37}$$

The time-domain filtered signal is obtained by an inverse FFT operation:

$$\mathbf{x}_f^{FDACA} = IFFT\left(\mathbf{X}_f^{FDACA}\right) \tag{38}$$

with

$$\hat{H}(k) = \frac{\bar{X}_r^H \, \bar{X}_s(k)}{|\bar{X}_r(k)|^2} \tag{39}$$

(^{H}) is the Hermitian operator, and $\bar{X}_r$ represents the spectral representation of the reference signal.

Once the static clutter suppression is performed, the filtered signals ($\mathbf{x}_f^{LMS}$, $\mathbf{x}_f^{ECA}$, and $\mathbf{x}_f^{FDACA}$) can be used to retrieve the cross-correlation function $\Psi_{CC}(\kappa, \nu)$, and to perform further detection processing stages.

3.3. Calculation Analysis of the Preprocessing

Since the aim of the averaging operation is the improvement of the received signals quality (SNR_r, CNR), an assessment of these two parameters after the averaging is required. Let's note $\text{SNR}_\text{r}^\text{out}$ and CNR^out the quality parameters of the resulting signals. The calculation of these two parameters passes through the calculation of the variances of the averaged signals $\bar{s}(n)$, $\bar{v}(n)$ and $\bar{w}(n)$ variances when N_s DVB-T symbols are considered.

Since the noise signals $v(i,n)$ and $w(i,n)$ follow centered Gaussian distributions of σ_v^2 and σ_w^2, respectively, the variances $\sigma_{\bar{v}}^2$ and $\sigma_{\bar{w}}^2$ of the averaged signals ($\bar{v}(n)$ and $\bar{w}(n)$) are given by:

$$\sigma_{\bar{v}}^2 = \frac{\sigma_v^2}{N_s} \tag{40}$$

and:

$$\sigma_{\bar{w}}^2 = \frac{\sigma_w^2}{N_s} \tag{41}$$

As mentioned in Section 2, the components of the DVB-T symbols are statistically independent, thus, the variance of the averaged DVB-T signal $\sigma_{\bar{s}}^2 = E\{\bar{s}(n)^2\}$ can be expressed as:

$$\sigma_{\bar{s}}^2 = \sigma_{p_c}^2 + \sigma_{\bar{p}_s}^2 + \sigma_{\bar{d}}^2 \tag{42}$$

with $\sigma_{\bar{p}_s}^2$ being the variance of the averaged scattered pilot signal $\bar{p}_s(n)$, and $\sigma_{\bar{d}}^2$ is the variance of the averaged data signal $\bar{d}(n)$. In the DVB-T standard, the scattered pilots pattern is repeated each four (04) DVB-T symbols, and the data subcarriers carry randomized QAM symbols, thus:

$$\sigma_{\bar{p}_s}^2 = \frac{1}{4}\sigma_{p_s}^2 \tag{43}$$

and:

$$\sigma_{\bar{d}}^2 = \frac{1}{N_s}\sigma_d^2 \tag{44}$$

as a result, the variance of the averaged DVB-T signal $\bar{s}(n)$ is given by:

$$\sigma_{\bar{s}}^2 = \sigma_{p_c}^2 + \frac{1}{4}\sigma_{p_s}^2 + \frac{1}{N_s}\sigma_d^2 \tag{45}$$

The signal-to-noise ratio of the averaged reference signal ($\text{SNR}_\text{r}^\text{out}$) can be expressed as:

$$\text{SNR}_\text{r}{}^\text{out} = |\xi|^2 \frac{\sigma_{\bar{s}}{}^2}{\sigma_{\bar{v}}{}^2} \tag{46}$$

substituting (40) and (45) in (46), we find:

$$\text{SNR}_\text{r}{}^\text{out} = |\xi|^2 \frac{N_s \times (\sigma_{p_c}^2 + \frac{1}{4}\sigma_{\bar{p}_s}^2) + \sigma_d^2}{\sigma_v^2} \tag{47}$$

which can be written as:

$$\text{SNR}_\text{r}{}^\text{out} = \text{SNR}_\text{r} \times (\gamma N_s + \lambda) \tag{48}$$

with the parameters γ and λ defined as:

$$\gamma = \frac{\sigma_{p_c}^2 + \frac{1}{4}\sigma_{p_s}^2}{\sigma_s^2} \tag{49}$$

$$\lambda = \frac{\sigma_d^2}{\sigma_s^2} \tag{50}$$

Similarly, the clutter-to-noise ratio of the averaged surveillance signal CNR^out can be expressed as:

$$\text{CNR}^\text{out} = \sum_{l=0}^{L-1} |h_l|^2 \frac{N_s \times (\sigma_{p_c}^2 + \frac{1}{4}\sigma_{\bar{p}_s}^2) + \sigma_d^2}{\sigma_w^2} \tag{51}$$

which can be written as:

$$\text{CNR}^{\text{out}} = \text{CNR} \times (\gamma N_s + \lambda) \tag{52}$$

The parameters γ and λ depend on the DVB-T mode (2 K, 8 K) and on the length of the guard interval length. In this paper, the 8 K mode is used with a guard interval $T_G = T_U/4$, thus, the values of the parameters γ and λ are given by:

$$\gamma \approx 0.083 \tag{53}$$

$$\lambda \approx 0.82 \tag{54}$$

Equations (48) and (52) illustrate the linear dependence of the averaged signals parameters (CNR^{out} and $\text{SNR}_{\text{r}}^{\text{out}}$) and the number of considered symbols N_s. To validate the retrieved expressions, Monte Carlo (MC) simulations have been carried out to simulate the averaging process and to characterize the averaged signals. Figures 6 and 7 represent the comparison of the theoretical expressions of Equations (48) and (52) from one side, and the results of the MC simulations from another side. One can remark the perfect match between the theoretical ($\text{SNR}_{\text{r}}^{\text{out}}$ (Th) and CNR^{out} (Th)) and the MC ($\text{SNR}_{\text{r}}^{\text{out}}$ (MC) and CNR^{out} (MC)) results which validates the retrieved expressions.
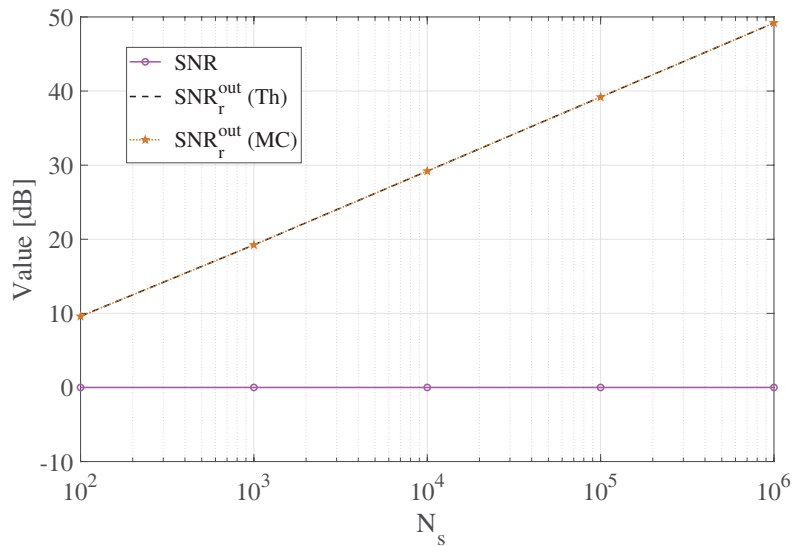

Figure 6. Impact of the proposed approach on the $\text{SNR}_{\text{r}}^{\text{out}}$ for in initial $\text{SNR}_{\text{r}} = 0$ dB.

Figure 6 represents the variation of the signal-to-noise ratio that characterizes the averaged reference signal ($\text{SNR}_{\text{r}}^{\text{out}}$) as a function of the number of considered DVB-T symbols N_s. In this case, the initial signal-to-noise ratio of the reference signal is set at $\text{SNR}_{\text{r}} = 0$ dB. The results show that if the number of considered symbols $N_s = 10^2$, the obtained value is $\text{SNR}_{\text{r}}^{\text{out}} = 10$dB. Therefore, an SNR_{r} improvement of 10 dB is granted. Moreover, if a larger number of symbols is considered such as $N_s = 10^4$, the SNR improvement is 30 dB which will improve the clutter estimation operation.

In Figure 7, the variation of the clutter-to-noise ratio of the averaged surveillance signal is presented as a function of the number of considered DVB-T symbols N_s. Here, the initial value of the CNR is 10 dB, and its improvement is linearly dependent on the value of N_s. For example, for $N_s = 10^2$ and $N_s = 10^4$, the CNR improvement is of 10 dB and 30 dB, respectively. These CNR improvements reflect an important noise reduction, and thus, a considerable improvement of the static estimation accuracy is expected.

At this point, the conclusion is that the larger the N_s is, the higher the improvement of SNRr and CNR is. In practice, an averaging over $N_s = 10^4$ that provides an improvement of 30 dB only requires an acquisition of 10 s duration. To enable the real-time processing possibility, the static clutter estimation can be performed in a primary stage, and the estimated clutter components can be used at each observation interval and periodically updated.
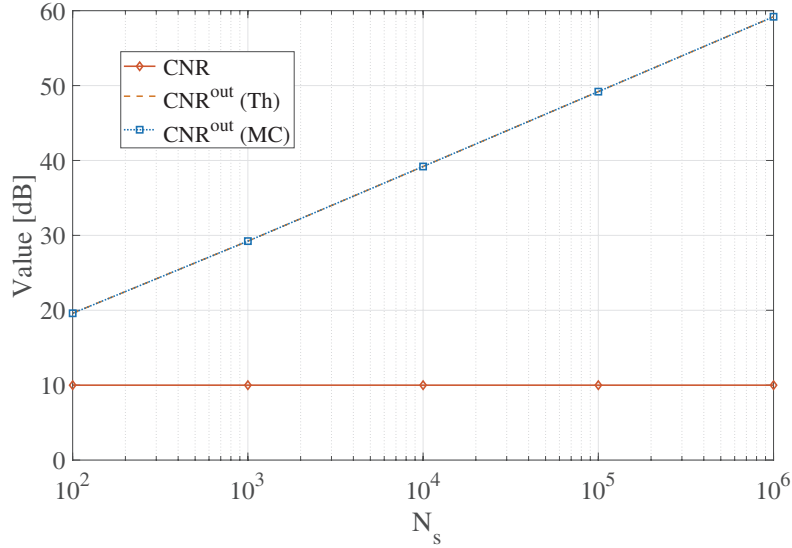
Figure 7. Impact of the proposed approach on the CNR^{out} for in initial CNR $= 10\,\text{dB}$.

4. SIMULATION RESULTS AND DISCUSSION

To evaluate the performances of the proposed signal conditioning approach, three (03) static clutter methods are considered and adapted to the use of averaged signals: LMS, ECA, and FDACA. The performance assessment is conducted through the consideration of two parameters: the normalized mean square error (NMSE) of the clutter estimation and the efficiency of the static clutter suppression in the resulting RDDs.

4.1. Evaluation of the Static Clutter Estimation Accuracy

The performance evaluation of the proposed approach in terms of accuracy of the clutter components estimation is quantified by the NMSE calculation, which is defined as follows:

$$\text{NMSE} = \frac{E\{|\hat{\mathbf{h}} - \mathbf{h}|^2\}}{E\{|\mathbf{h}|^2\}} \tag{55}$$

To obtain the performance results in terms of NMSE, Monte Carlo (MC) simulations have been carried out. Table 2 summarizes the main parameters used for simulation.

To evaluate the performance improvement brought to the LMS method when averaged signals are employed, we consider a scenario with a direct-path component $h_0 = 1$ and a reference signal SNR of

Table 2. Simulation main parameters.

Parameter	Value
Number of MC trials	1000
Static clutter vector length (L)	100
Symbols Number N_s	10^4
Clutter components indexes interval	$l \in [0; L-1]$
clutter components amplitudes interval	$|h_l| \in [0; 1]$
CNR	$20\,\text{dB}$
SNR_r interval	$[0\text{--}30]\,\text{dB}$
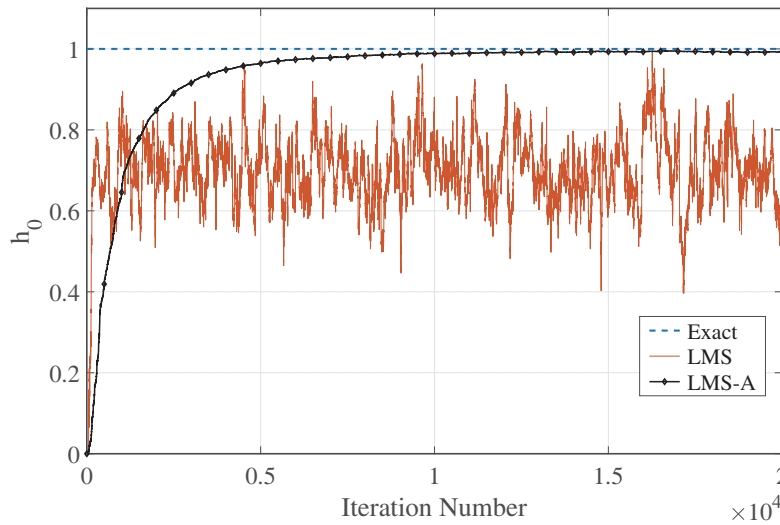
Figure 8. Comparison of the LMS convergence rate with the proposed LMS-A for $\text{SNR}_r = 5\,\text{dB}$.

$5\,\text{dB}$. Figure 8 shows the value of the estimated component $\hat{h}_0$ as a function of the iteration index for the traditional approach and the proposed one. The results show that the use of noisy signals leads to an inaccurate estimation of the clutter component with a significant fluctuation. However, the use of the averaged signals gives a correct estimation of h_0 and a fast convergence rate.

In Figure 9, the NMSE of the clutter components estimation as a function of the reference signal SNR is represented for the LMS method using raw and averaged signals. The results show that for $\text{SNR}_r < 15\,\text{dB}$, the NMSE of the proposed approach is 10^4 lower that the use of raw signals. And for $\text{SNR}_r > 15\,\text{dB}$, the NMSE is 10^3 lower. In both cases, a significant NMSE reduction is achieved which will lead to an efficient static clutter suppression and reduces the residual clutter.
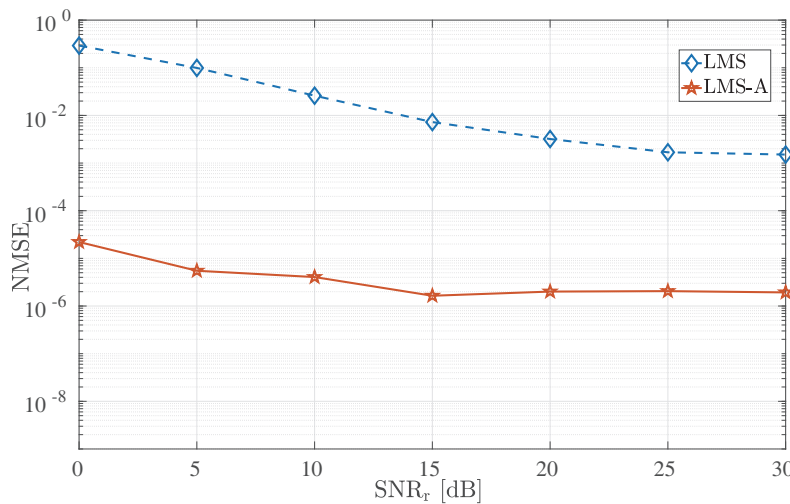

Figure 9. NMSE of the proposed method compared to the conventional one.

Figure 10 represents the NMSE of two variants of the ECA method: ECA [20] and ECA-B [30] in addition to the ECA with conditioned signals. As the case of the LMS algorithm, an NMSE reduction of at least 10^3 is achieved for the considered SNR_r range.

Figure 11 shows the NMSE for the FDACA and the same method when averaged signals are used (FDACA-A). In this case, the NMSE reduction is larger than the first two methods; a factor of 10^5 is
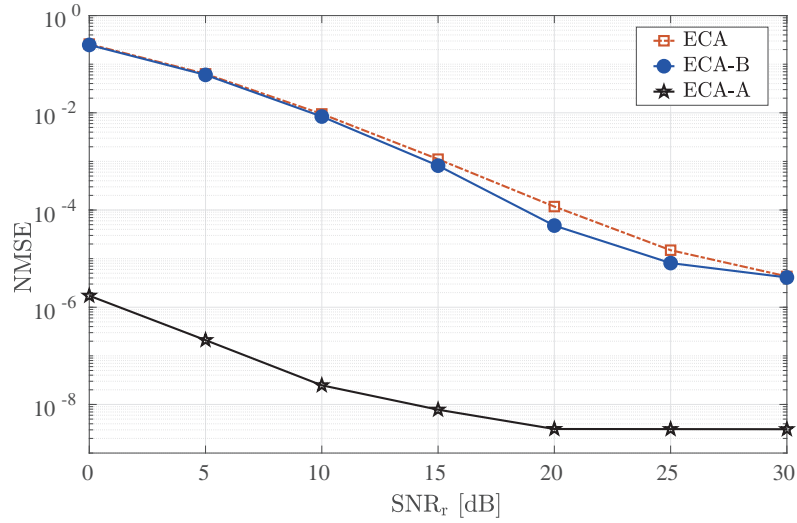
Figure 10. Different ECA versions NMSE function of $\mathrm{SNR_r}$ compared to the proposed method.
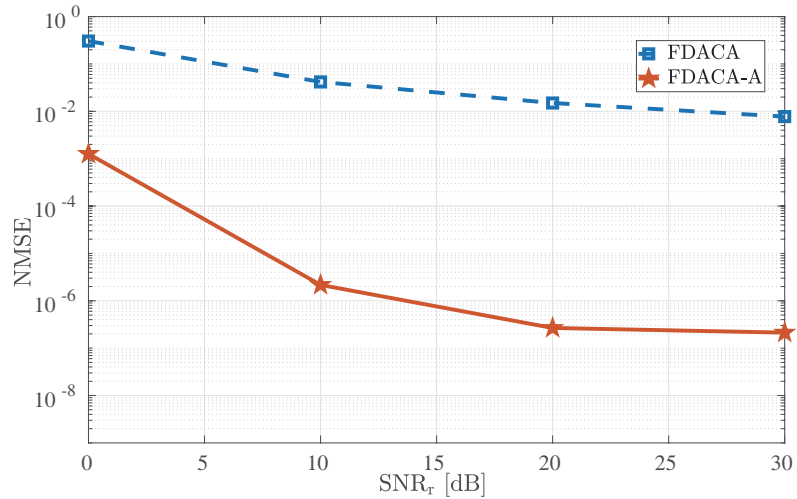

Figure 11. Comparison between the NMSE evolution function of the $\mathrm{SNR_r}$ for the proposed method FDACA-A and the classic FDACA.

achieved which reveals the important improvement brought to the FDACA when the proposed approach is used.

4.2. Evaluation of the Static Clutter Suppression Efficiency

The previously demonstrated NMSE reduction certainly leads to a significant improvement of the static clutter suppression process. This improvement can be highlighted through the study of the resulting RDD results before and after the application of the proposed method. In order to do so, we consider one simulated data set of length 0.05 seconds with randomly generated clutter components. Then, the RDDs are calculated for the considered cases. The results are shown in two profiles of the RDDs: the profile of the direct-path component ($R_b = 0$) and the profile of the zero-Doppler axis ($f_d = 0$).

Figures 12(a) and 12(b) illustrate the RDD results for the classic LMS method and the proposed method that uses averaged signals (LMS-A). Figure 12(a) shows the impact of the static clutter on the RDD through the high level of the sidelobes around $f_d = 0$ Hz, which induces a high noise-floor level that masks the target echoes. The results after applying the LMS method show that the main lobe
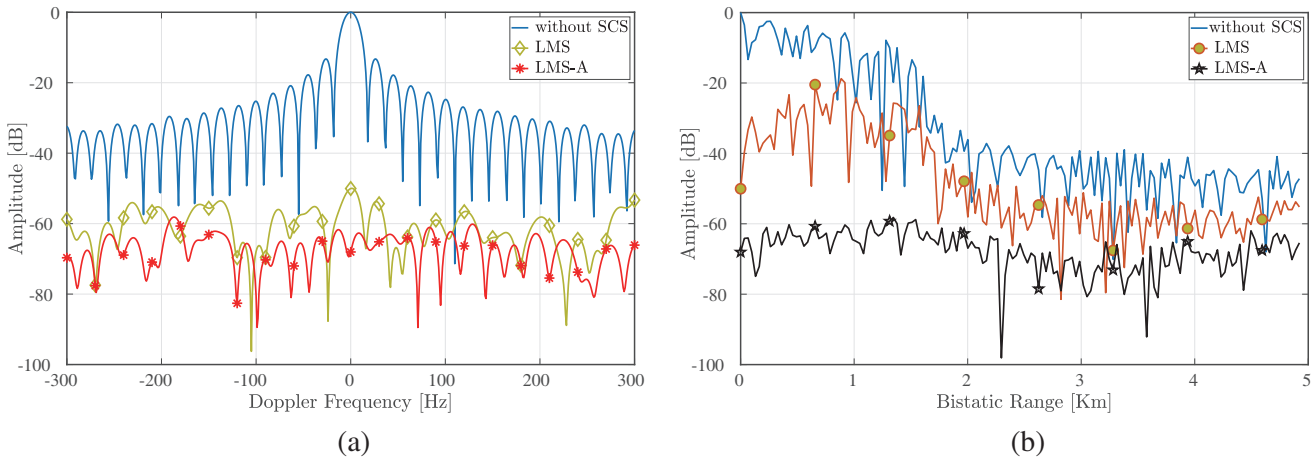
Figure 12. RDD profiles (a) direct-path and (b) zero-Doppler for the LMS method.

is reduced by $-50\,\mathrm{dB}$, and the noise-floor is also significantly reduced. A more important reduction is then obtained when the LMS-A is employed. In this case, the level at zero-Doppler reaches $-65\,\mathrm{dB}$. The RDD profile for the zero-Doppler axis is represented in Figure 12(b), where the same remarks about the efficiency of the LMS-A are again validated.

In Figures 13(a) and 13(b), the RDDs resulting from the application of the ECA method are illustrated. The zero-range profile presented in Figure 13(a) shows that the conventional ECA methods can achieve a static clutter suppression of $40\,\mathrm{dB}$. In addition, this level can be highly improved to reach $-70\,\mathrm{dB}$ when the conditioned signals are employed (ECA-A). Figure 13(b) provides the zero-Doppler profile, and it shows the efficiency of the use of the averaged signals associated with the ECA method.
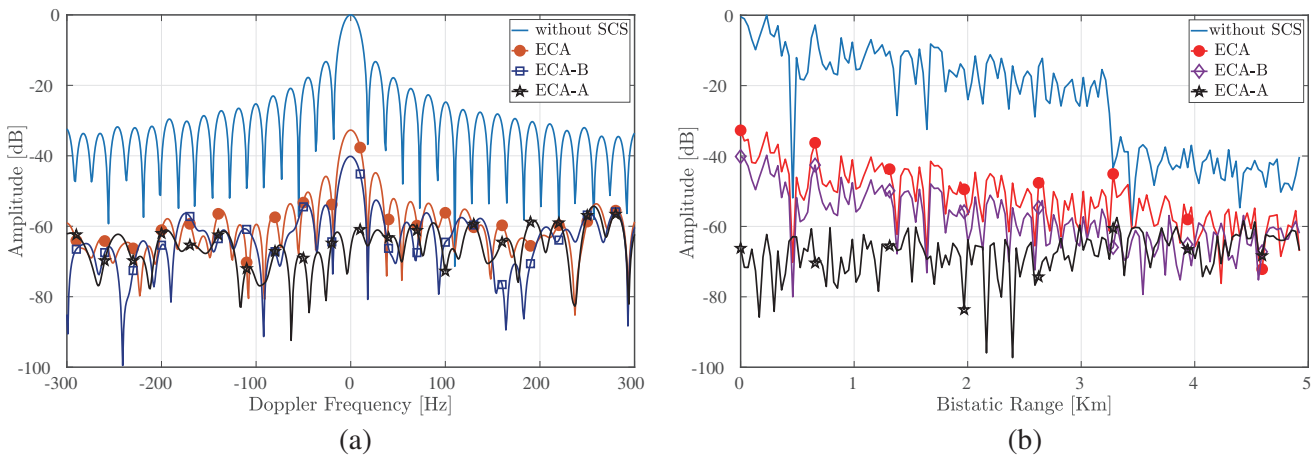

Figure 13. RDD profiles (a) direct-path and (b) zero-Doppler for the ECA method.

Figures 14(a) and 14(b) show the RDDs resulting from the application of the FDACA static clutter suppression method. We can notice that the clutter suppression is performed with a high efficiency for the FDACA-A ($-70\,\mathrm{dB}$) compared to the classical FDACA ($-40\,\mathrm{dB}$).

Table 3 illustrates the comparison between the processing time of the considered methods and their corresponding improved versions adapted to the new approach. The signals length used in this operations is $N_s = 10^4$ DVB-T symbols, and the simulated clutter vector length is $L = 100$. A computer with i5 processer and $8\,\mathrm{GB}$ of RAM is employed. It confirms that the new proposed approach improves the speed of the conventional algorithms because of the reduction of the signals length, by dealing
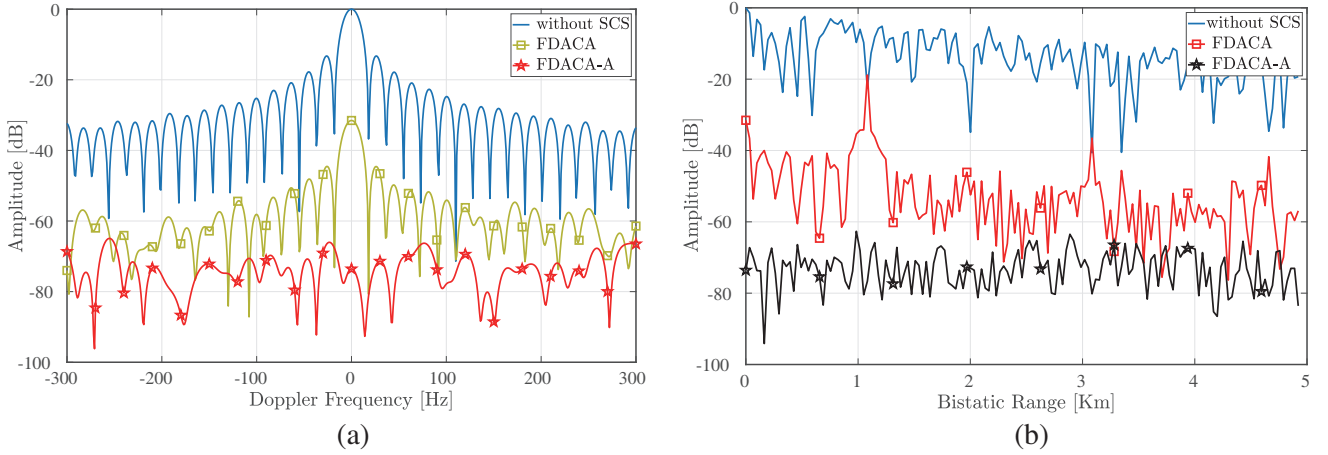
Figure 14. RDD profiles (a) direct-path and (b) zero-Doppler for the FDACA method.

Table 3. The processing time of different methods for $N_s = 10^4$ DVB-T symbol.

Conventional Method	Processing time [s]	Proposed Approach	Processing time [s]
LMS	530.1	LMS-A	1.7
ECA	65.8	ECA-A	2.6
ECA-B	13.7		
FDACA	19.3	FDACA-A	0.5

with one DVB-T symbol length instead of considering the full received signals during the static clutter estimation stage.

5. EXPERIMENTAL RESULTS

In this section, the real data results are presented. The measurements have been conducted using the experimental bench illustrated in Figure 15, where two Yagi-Uda directive antennas, both have a direct Gain of 11 dB, have been used together with a USRP X310 board. The reception site is located at the Royal Military Academy (RMA) of Brussels.

As shown in Figure 16, the considered transmitter of opportunity is located at the Finance Tower with a distance of 2.3 km from the reception site. The considered surveillance sector is chosen toward the Brussels Zaventem airport with a distance of 8.5 km from the RMA.

The main characteristics of the Finance Tower Transmitter are presented in Table 4.

Table 4. Transmitted DVB-T signal main characteristics.

Parameter	Value
Mode	8 K
Transmission power	10 KW
Carrier frequency	754 MHz
DVB-T sampling frequency	64/7 MHz
USRP sampling Frequency	10 MHz
QAM modulation	16 QAM

Figure 15. Experimental bench used for data collection.

Figure 16. Reception configuration.

As described in Section 5, the collected data will undergo two signal processing stages. The first stage is related to the estimation of the static clutter components, and the second stage concerns the target detection after applying the static clutter suppression (SCS). To achieve an improvement of $40\,\mathrm{dB}$ of the CNR in the surveillance signal, the clutter estimation stage employs 10^5 DVB-T symbols which is about 100 seconds of data recording. During the acquisition, no moving targets are present in the surveillance sector, and thus the received surveillance signal exclusively contains reflected echoes from the static scatterers of the scene. For the second stage which concerns the target detection, the data recording is manually started when the airplanes enter the surveillance sector for landing or taking-off maneuvers at the Zaventem airport. For this stage, data are time-divided into blocks of 0.1 seconds which is sufficient to ensure a considerable coherent integration gain without causing a range walk.
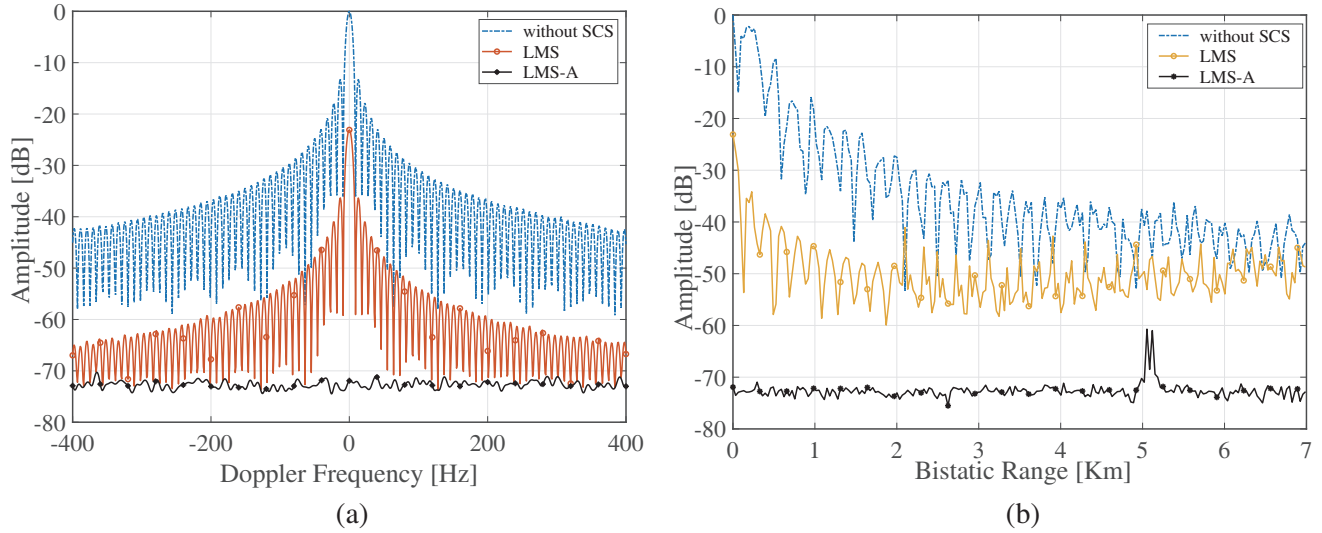
Figure 17. RDD profiles (a) direct-path and (b) zero-Doppler for the LMS method.
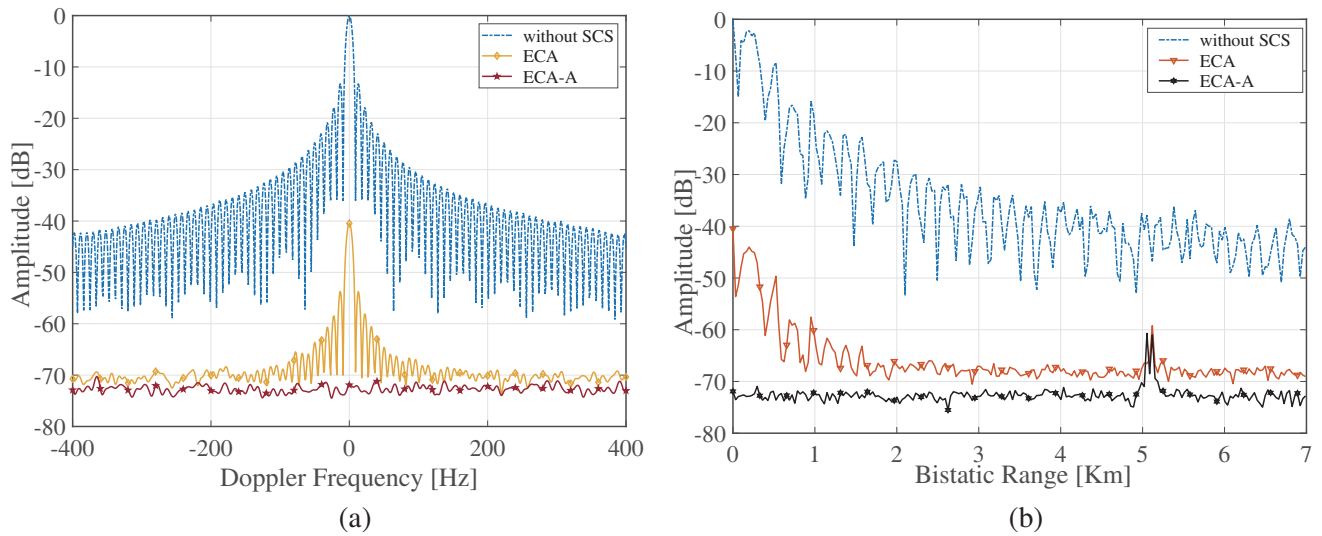

Figure 18. RDD profiles (a) direct-path and (b) zero-Doppler for the ECA method.

First, the efficiency of the static clutter suppression is evaluated. Figures 17, 18, and 19 represent both the Doppler profile at the zero bistatic range and the range profile at the zero Doppler axis of the summed RDDs obtained from real-data of the considered methods for static clutter suppression. The results show the profiles before (LMS, ECA, FDACA) and after (LMS-A, ECA-A, FDACA-A) using the proposed approach that improves the CNR and SNR_r levels. It can be easily noticed that the real data results fit to the earlier simulation results. The figures show that the efficiency of the SCS by the conventional methods is considerably improved when the averaged signals are employed. As a result, the residual static clutter reaches the noise level, and consequently, the moving targets can be easily detected in the next stage.

It is worth to mention that for the range profiles: The peak at 5 km corresponds to the target echo when its Doppler frequency is close to zero. For what is related to the fact that the range profiles are similitude for LMS-A, ECA-A, and FDACA-A, and the similarity is because the same dataset has been used for all the methods, and since the signals have been perfectly conditioned, the result should be the same.
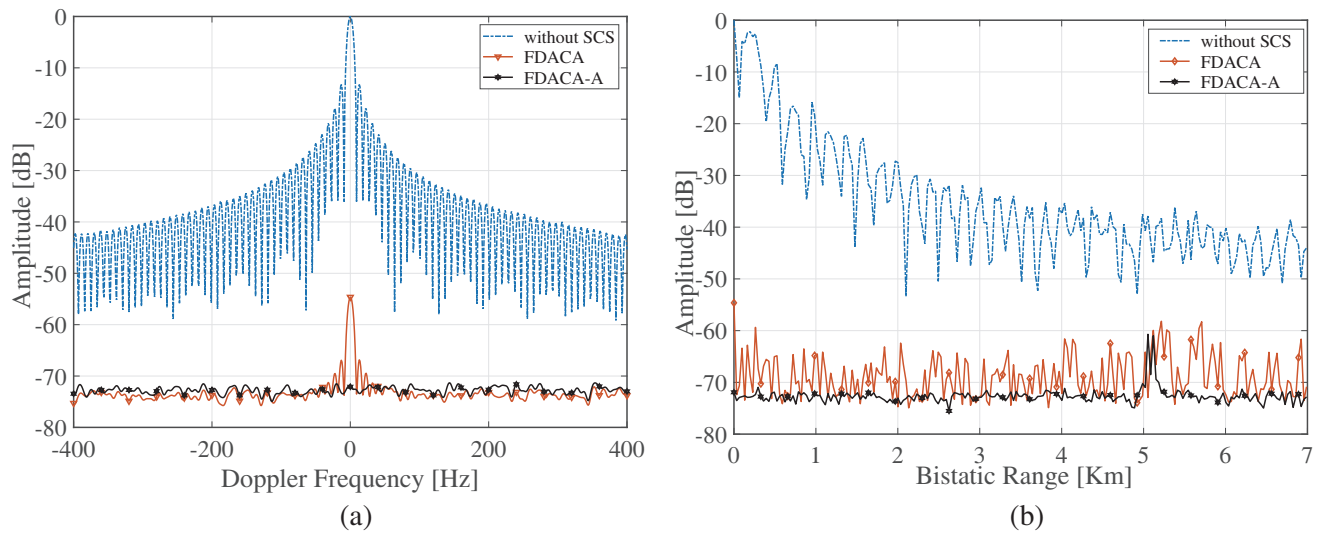
Figure 19. RDD profiles (a) direct-path and (b) zero-Doppler for the FDACA method.
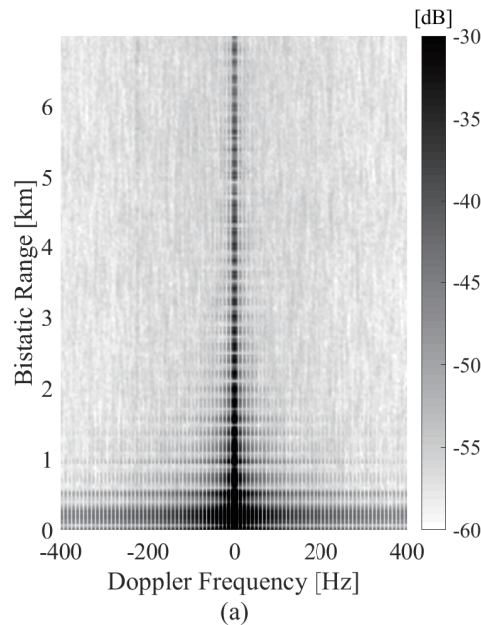

Figure 20. RDDs (a) Without statique clutter suppression.

Second, the real data containing target echoes are processed to emphasize the impact of the proposed approach on the detection efficiency: a sequence with a duration of 15 seconds is employed for this aim. The full-size data are divided for batches of 0.1 seconds duration. The obtained batches are processed for SCS, and a range-Doppler diagram is calculated for each batch. The resulting RDDs are summed to obtain a full target track over the observation time.

Figures 20–23 show the summed range-Doppler diagrams before applying the static clutter suppression, after employing the conventional methods (LMS, ECA, FDACA), and after using the proposed approach (LMS-A, ECA-A, FDACA-A). Figure 20(a) shows the summed RDDs when no SCS is applied: one can notice that the static clutter around zero Doppler masks the target track. When the conventional methods are applied, the results are shown in Figures 21(b), 22(c), and 23(d). The target track can be clearly distinguished. It corresponds to an airplane with a bistatic range varying between
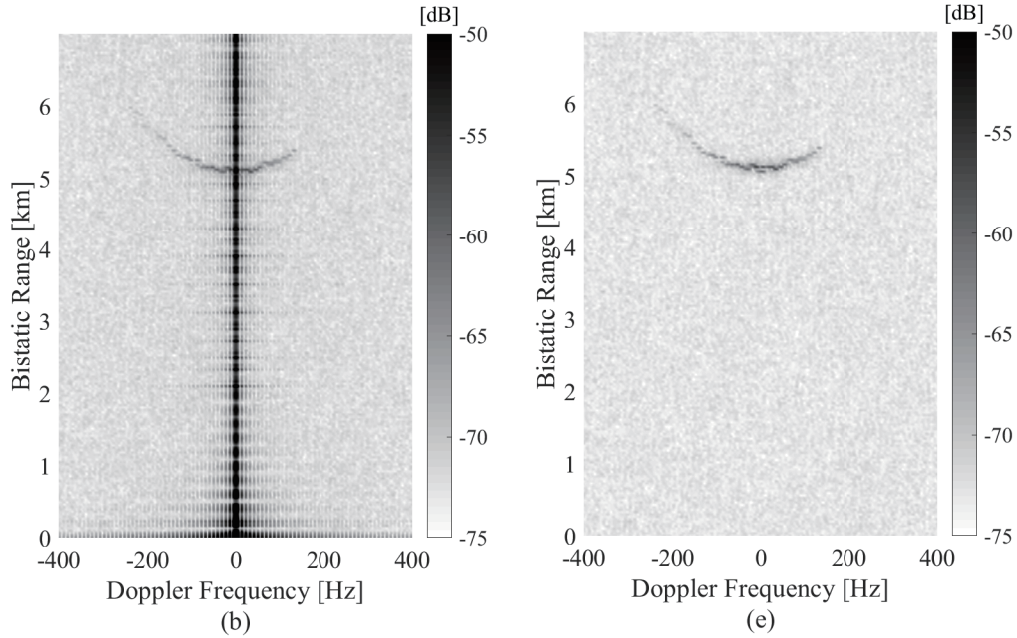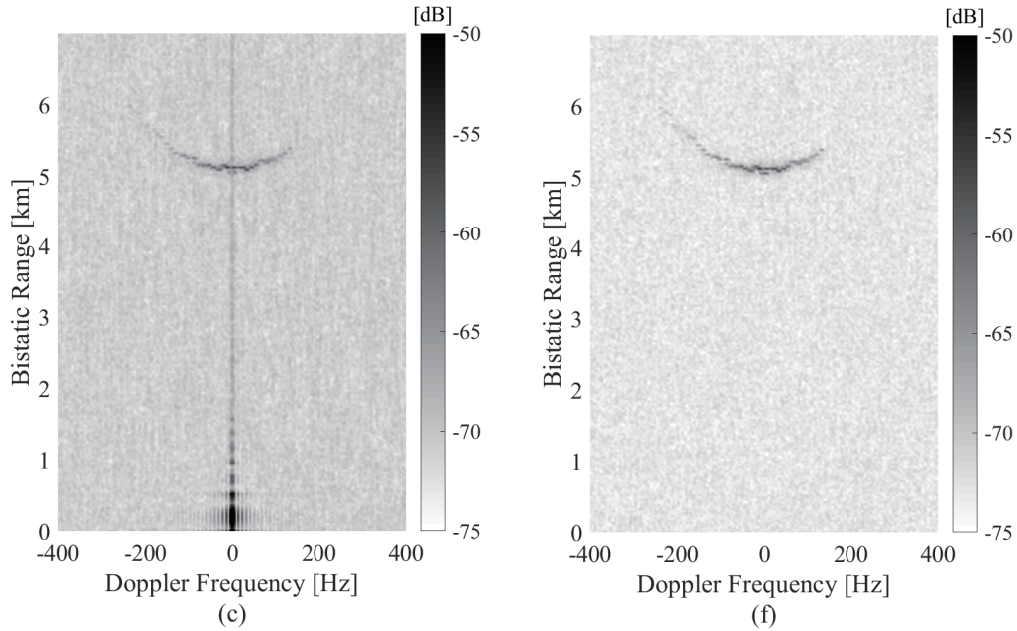
Figure 21. RDDs (b) LMS Method, (e) LMS-A method.

Figure 22. RDDs (c) ECA method, (f) ECA-A method.

05 km and 06 km. For the Doppler shift it is between $-200\,\text{Hz}$ and $+200\,\text{Hz}$. Although the target track is distinguishable from the noise level, a residual clutter remains present when conventional methods are applied.

Figures 21(e), 22(f), and 23(g) present the resulting summed RDDs corresponding to the use of the proposed approach of signal quality improvement (LMS-A, ECA-A, FDACA-A). The results show that the static clutter suppression is perfectly executed since no residual clutter is present. It shows again the importance of the improving the signals quality before applying the SCS. These results, obtained through the real data processing, validate the theoretical and the simulation results previously obtained.
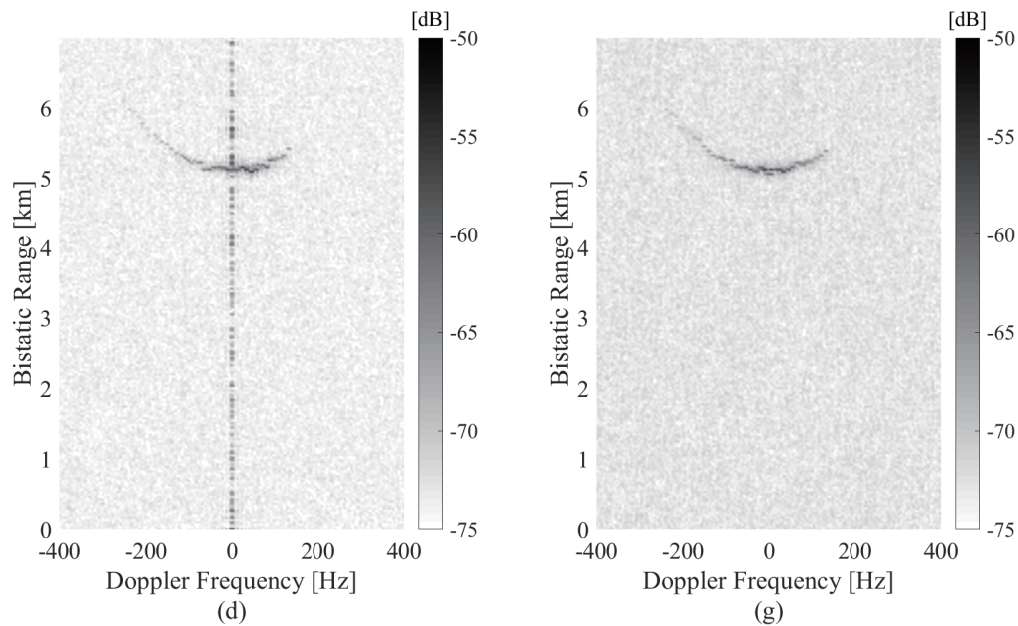
Figure 23. RDDs (d) FDACA method, (g) FDACA-A method.

Consequently, improving the quality of the reference and the surveillance is a pivot stage to enhance both the static clutter suppression efficiency and the target detection.

In addition, as mentioned in Section 3, the proposed approach includes two stages, and the clutter components estimation is performed when there is no target. Then, these estimated components are used to suppress the static clutter when there is a target. Thus, a target with a near-zero Doppler will not be suppressed since there was now clutter at this cell during the estimation stage.

Another point is also worth to be clarified. The Doppler resolution depends on the integration time T_{int}. In fact, this resolution is given by $\Delta f = 1/T_{int}$. In our case ($T_{int} = 0.1\,\mathrm{s}$), the Doppler resolution is of $\Delta f = 10\,\mathrm{Hz}$. As a result, a peak at zero-Doppler can be actually characterized by a Doppler shift between $[-5\,\mathrm{Hz},\, 5\,\mathrm{Hz}]$ and not only a target with perfect zero-Doppler.

6. CONCLUSION

In this paper, a new approach of the static clutter components estimation and suppression is proposed for passive radar systems employing DVB-T transmitters as illuminators of opportunity. The specific structure of the received signals is exploited to achieve a low computation load by taking the average of the received DVB-T symbols; as a result, the noise effect is also reduced. The considered simulation scenarios include three static clutter suppression methods: LMS, ECA, and FDACA. The results show that, by considering the proposed method, the NMSE of the clutter components estimation is reduced by at least a factor 10^3, and that the static clutter suppression efficiency is improved by at least 15 dB. Since the static clutter is time-invariant, the clutter estimation stage can be performed separately prior to the detection operation, and the efficiency of the proposed approach is verified using the real dataset collected by an experimental bench, the static clutter rejection is strongly ensured by the proposed algorithms compared with the conventional methods.

REFERENCES

1. Eaves, J. and E. Reedy, *Principales of Modern Radar*, Springer Science & Business Media, 2012.
2. Griffiths, H., "Passive bistatic radar, in: Academic press library in signal processing," *Elsevier*, Vol. 2, 813–855, 2014.

3. Willis, N., *Bistatic Radar*, SciTech Pub., Raleigh, NC.

4. Cherniakov, M. A., *Bistatic Radar: Emerging Technology*, John Wiley and Sons Chichester, UK, 2008.

5. Mahfoudia, O., "Dvb-t based bistatic passive radars in noisy environments," Ph.D. Thesis, 2017.

6. Malanowski, M., K. Kulpa, J. Kulpa, P. Samczynski, and J. Misiurewicz, "Analysis of detection range of FM-based passive radar," *IET Radar, Sonar & Navigation*, Vol. 8, No. 2, 153–159, 2014.

7. Zemmari, R., U. Nickel, and W.-D. Wirth, "Gsm passive radar for medium range surveillance," *2009 European Radar Conference (EuRAD), IEEE*, 49–52, 2009.

8. Griffiths, H. and C. Baker, "Passive coherent location radar systems. Part 1: Performance prediction," *IEE Proceedings-Radar, Sonar and Navigation*, Vol. 152, No. 3, 153–159, 2005.

9. Malanowski, K. and M. et Kulpa, "Deux m'ethodes de localisation de cible dans un radar passif multistatique," *Transactions IEEE sur Les Systèmes Aérospatiaux et Électroniques*, Vol. 48, No. 1, 572–580, 2012.

10. Liu, J., H. Li, and B. Himed, "On the performance of the cross-correlation detector for passive radar applications," *Signal Processing*, Vol. 113, 32–37, 2015.

11. Liu, J., H. Li, and B. Himed, "Analysis of cross-correlation detector for passive radar applications," *2015 IEEE Radar Conference (RadarCon), IEEE*, 0772–0776, 2015.

12. Mahfoudia, O., F. Horlin, and X. Neyt, "Performance analysis of the reference signal reconstruction for DVB-T passive radars," *Signal Processing*, Vol. 158, 26–35, 2019.

13. Palmer, J. E., H. A. Harms, S. J. Searle, and L. Davis, "DVB-T passive radar signal processing," *IEEE Trans. Signal Process*, Vol. 61, No. 8, 2116–2126, 2013.

14. Harms, L. M. D. H. A. and J. Palmer, "Understanding the signal structure in DVB-tsignals for passive radar detection," *2010 IEEE Radar Conference*, 532–537, 2010.

15. Plotka, M., M. Malanowski, P. Samczynski, K. Kulpa, and K. Abratkiewicz, "Passive bistatic radar based on VHF DVB-T signal," *2020 IEEE International Radar Conference (RADAR), IEEE*, 596–600, 2020.

16. Daun, M., U. Nickel, and W. Koch, "Tracking in multistatic passive radar systems using DAB/DVB-T illumination," *Signal Processing*, Vol. 92, No. 6, 1365–1386, 2012.

17. Venu, D. and N. K. Rao, "A computational statistics review for low complexity clutter cancellation for passive bi-static radar," *Methodologies and Applications of Computational Statistics for Machine Intelligence*, 142–163, 2021.

18. Cardinali, R., F. Colone, L. Ferretti, Chiara, and P. francesco, "Comparison of clutter and multipath cancellation techniques for passive radar," *2007 IEEE Radar Conference, IEEE*, 469–474, 2007.

19. Tang, B., J. Li, Y. Zhang, and J. Tang, "Design of mimo radar waveform covariance matrix for clutter and jamming suppression based on space time adaptive processing," *Signal Processing*, Vol. 121, 60–69, 2016.

20. Colone, R. C. F. and P. Lombardo, "Cancellation of clutter and multipath in passive radar using a sequential approach," *2006 IEEE Conference on Radar, IEEE*, 393–399, 2006.

21. Bolvardi, H., M. Derakhtian, A. Sheikhi, "Dynamic clutter suppression and multitarget detection in a DVB-T-based passive radar," *IEEE Transactions on Aerospace and Electronic Systems*, Vol. 53, No. 4, 1812–1825, 2017.

22. Kulpa, K., "The clean type algorithms for radar signal processing," *2008 Microwaves, Radar and Remote Sensing Symposium, IEEE*, 152–157, Sep. 2008.

23. Mahfoudia, O., F. Horlin, and X. Neyt, "Pilot-based detection for DVB-T passive coherent location radars," *IET Radar, Sonar & Navigation*, Vol. 14, No. 6, 845–851, 2020.

24. Attalah, M. A., T. Laroussi, F. Gini, and M. S. Greco, "Fast block lms algorithm for interference cancellation in DVB-T based passive bistatic radar," *2017 5th International Conference on Electrical Engineering-Boumerdes (ICEE-B), IEEE*, 1–5, 2017.

25. Wang, Y. M. K., R. Tao, and T. Shan, "Adaptive multipath cancellation algorithm in passive radar," *2006 CIE International Conference on Radar, IEEE*, 1–4, Oct. 2006,

26. Palmer, J. E. and S. J. Searle, "Evaluation of adaptive filter algorithms for clutter cancellation in passive bistatic radar," *2012 IEEE Radar Conference, IEEE*, 0493–0498, May 2012.

27. Meller, M. and S. Tujaka, "Processing of noise radar waveforms using block least mean squares algorithm," *IEEE Transactions on Aerospace and Electronic Systems*, Vol. 48, 749–761, Jan. 2012.

28. Xiang, Y. Z. M., X. Lu, and Y. Zhao, "Block nlms cancellation algorithm and its real-time implementation for passive radar," *IET International Radar Conference 2013, Institution of Engineering and Technology*, 0431–0431, 2013.

29. Del Rey-Maestre, N., M.-P. Jarabo-Amores, J.-L. B'arcena-Humanes, D. Mata-Moya, and P. Gomez-del Hoyo, "Eca filter effects on ground clutter statistics in DVB-T based passive radar," *2018 26th European Signal Processing Conference (EUSIPCO), IEEE*, 1227–1231, 2018.

30. Colone, P. L. F., D. W. OHagan, and C. J. Baker, "A multistage processing algorithm for disturbance removal and target detection in passive bistatic radar," *IEEE Transactions on Aerospace and Electronic Systems*, Vol. 45, 698–722, Apr. 2009.

31. Schwark, C. and D. Cristallini, "Advanced multipath clutter cancellation in OFDM-based passive radar systems," *2016 IEEE Radar Conference (RadarConf), IEEE*, 1–4, 2016.

32. Zhao, D., J. Wang, G. Chen, J. Wang, and S. Guo, "Clutter cancellation based on frequency domain analysis in passive bistatic radar," *IEEE Access*, Vol. 8, 43956–43964, 2020.

33. Schwark, C. and OFDM-based passive radar systems," *2016 IEEE Radar Conference (RadarConf), IEEE*, 1–4, May 2016.

34. Mahfoudia, O., F. Horlin, and X. Neyt, "On the static clutter suppression for the DVB-T based passive radars," *2017 XXXIInd General Assembly and Scientific Symposium of the International Union of Radio Science (URSI GASS), IEEE*, 1–4, 2017.

35. Berthillot, C., A. Santori, O. Rabaste, D. Poullin, and M. Lesturgie, "DVB-T airborne passive radar: clutter block rejection," *2019 International Radar Conference (RADAR), IEEE*, 1–5, 2019.

36. Palmer, J. E., H. A. Harms, S. J. Searle, and L. Davis, "DVB-T passive radar signal processing," *IEEE transactions on Signal Processing*, Vol. 61, No. 8, 2116–2126, 2012.

37. Ladebusch, U. and C. A. Liss, "Terrestrial DVB (DVB-T): A broadcast technology for stationary portable and mobile use," *Proceedings of the IEEE*, Vol. 94, No. 1, 183–193, 2006.

38. Institute, E. T. S., "Digital video broadcasting (DVB): Framing structure, channel coding and modulation for digital terrestrial television," The Institue, 2009.